

# Performance analysis of MAPbI<sub>3</sub> based perovskite solar cells employing diverse charge selective contacts: Simulation study

Yassine Raoui<sup>1,3</sup>, Hamid Ez-Zahraouy<sup>3</sup>, Najim Tahiri<sup>3</sup>, Omar EL Bounagui<sup>4</sup>, Shahzada Ahmad<sup>1,2</sup>, Samrana Kazim<sup>1,2\*</sup>

<sup>1</sup>BCMaterials, Basque Center for Materials, Applications and Nanostructures, Bld. Martina Casiano, UPV/EHU Science Park, Barrio Sarriena s/n, 48940 Leioa, Spain

<sup>2</sup> IKERBASQUE, Basque Foundation for Science, Bilbao, 48013, Spain.

<sup>3</sup>Laboratory of Condensed Matter and Interdisciplinary Sciences, Faculty of Sciences, Mohammed V University, Rabat, Morocco

<sup>4</sup>Physics Department, Mohammed V University in Rabat, Morocco

\* E-mail address: [samrana.kazim@bcmaterials.net](mailto:samrana.kazim@bcmaterials.net)

## ABSTRACT

The rapid development in the field of organo-metal halide perovskite solar cells (PSCs) has led to the report of power conversion efficiency of >25%. However, their large-scale deployment and possible commercialization endeavor are currently limited due to the presence of high-temperature processed electron transport material (ETM) such as TiO<sub>2</sub> and the expensive hole transport material (HTM) in the state-of-the-art devices. By employing Solar Cell Capacitance Simulator (SCAPS)-1D, we attempted to propose low cost charge selective materials as ETM and HTM, which can deliver high photovoltaic performance. For this, the evaluation of TiO<sub>2</sub>, ZnO and SnO<sub>2</sub> as ETMs was validated. Besides this, the role of thickness of ETMs was also investigated in a perovskite solar cells using CH<sub>3</sub>NH<sub>3</sub>PbI<sub>3</sub> perovskite as light harvester and Spiro-OMeTAD as HTM. Our simulation results showed that 90nm of SnO<sub>2</sub> layer outperform as ETM for device fabrication. Furthermore, in our pursuit to avoid the usage of Spiro-OMeTAD, different organic and inorganic HTMs (P3HT, CuSbS<sub>2</sub>, Cu<sub>2</sub>O, CuSCN) have been investigated, and more importantly the HTM thickness was optimized for high performance solar cells. We have found that by using the configuration of FTO/SnO<sub>2</sub> (90 nm)/MAPbI<sub>3</sub>/CuSCN (100 nm)/Au can yield a PCE of 26.74% and V<sub>oc</sub> of 1180mV and FTO/SnO<sub>2</sub> (90 nm)/MAPbI<sub>3</sub>/Spiro-OMeTAD (100 nm)/Au. The role of metal cathode work function was also studied to replace the expensive gold (Au) electrode.

Key words: perovskite; solar cells; charge selective contacts; hole transporting materials; Electron transporting materials.

## 1. Introduction

Organic–inorganic halide perovskites have received significant attention due to their extraordinary and tunable electro-optical properties, leading to improve performance in solar cells and light emitting devices. These materials are well known for over a decade; however, Miyasaka et al in 2009, mentioned its first usage in solar cells (Kojima et al., 2009).

These materials can be represented by a general formula  $ABX_3$ , where A is an organic methylammonium ( $CH_3NH_3^+$ ) ion (Kazim et al., 2014) or formamidinium ( $NH=CHNH_3^+$ ) ion (Eperon et al., 2014; Koh et al., 2013; Salado et al., 2019) B is inorganic cation  $Pb^{2+}$ ,  $Sn^{2+}$ , and X can be a halogen ion,  $I^-$ ,  $Br^-$ , or  $Cl^-$ .

The remarkable performance of three-dimensional  $ABX_3$  perovskites in solar cells was due to their panchromatic light absorption throughout the visible and near infrared spectrum, low exciton binding energy ( $\sim 2$  meV), direct band gap, (Lin et al., 2015) long diffusion length, high charge carrier mobility, which makes them ideal photovoltaic materials (Stoumpos et al., 2013) with controlling the quality of perovskite film by different methods can decrease the defect density to improve the photovoltaic parameters (Sun et al., 2018; Wang et al., 2018). Owing to these unique characteristics, the certified power conversion efficiency (PCE) of 25.2 % was reported (NREL, 2019). Among the best efficiencies in PSCs reported till date are based on  $TiO_2$  as ETM. However,  $TiO_2$  needs to be annealed at high temperature ( $500^\circ C$ ) to acquire the crystalline rutile phase (Burschka et al., 2013; Salado et al., 2018, 2017) which inhibits the application of PSCs in flexible devices. Moreover,  $TiO_2$  has low electron mobility (Guo et al., 2015) and is UV un-stable (Leijtens et al., 2013). To avoid these drawbacks, Liu et al. used a low-temperature solution-processed based ZnO as ETM and they measured a PCE of 15.7 % in planar PSCs (Liu and Kelly, 2014). These results showed new directions to replace  $TiO_2$  by other metal oxide as ETM for high efficiency PSCs. In 2015, Ke et al. demonstrated a PCE of 16.02 %, when low temperature solution-processed  $SnO_2$  layer was used as an ETM in a normal planar structured PSCs with less hysteresis (Ke et al., 2015). In another report,  $SnO_2$  has been used as an efficient ETM in planar PSCs synthesized using low temperature ALD method, yielding a PCE of 18% along with no hysteresis (Baena et al., 2015). The recent results using  $SnO_2$  as an ETM in PSCs showed high performance similar to  $TiO_2$  and ZnO in planar architecture, with  $V_{oc}$  of 1090 mV and PCE of 20.3% (Anaraki et al., 2016) and also  $SnO_2$  have received more attention due to its electronic structure (Salmani et al., 2018). However, these promising PSCs still suffer from the use of small organic molecule based Spiro-OMeTAD as HTM. To work as an efficient HTM, this Spiro-OMeTAD needs dopant and additives such as hygroscopic LiTFSI salt and *t*-BP, which makes the perovskite solar cells unstable (Reyna et al., 2016). Besides, degradation of perovskite in the presence of doped Spiro-OMeTAD, the other reasons includes 33.9% of the total device cost occurs due to the HTM synthesizing steps along with cost ineffective gold (Au) working as cathode in devices. (Gong et al., 2015). To replace Spiro-OMeTAD, several other organic small molecules, polymers, inorganic p-type semiconductors and organometallic complexes have been employed as HTM in PSCs and exhibited significant PV performance. (Calió et al., 2017, 2016a, 2016b; Cogal et al., 2018; Di et al., 2018). However, in terms of atmospheric stability, few of them were found to be encouraging.

Recently, Cu-Based ternary chalcogenide semiconductors described by a general formula  $Cu_aBX_b$  ( $B=Sn, Sb, Bi$  and  $X=Se, Te, S$ ) are showing more attention as new HTMs in thin film solar cells (Garza et al., 2011), such as  $CuSbS_2$  is from the family of abundant and cheap sulfates

in nature (Zhou et al., 2009). Similarly, others Cu based inorganic HTMs includes Cu<sub>2</sub>O (Yu et al., 2016), CuI and CuSCN (Hossain et al., 2015; Qin et al., 2014) demonstrated promising HTMs in PSCs to enhance the performance and importantly due to their low cost. These inorganic HTMs have high conductivity and high carrier mobility as compared to organic HTMs and can be used without doping but still need more investigation with the best electron selective layer for efficient PSCs .

To address these challenges which have hindered the commercialization of PSCs, in the present work, we have used simulation programme named (Solar cell capacitance simulator) SCAPS for the screening of the HTMs which can be tested experimentally in optimized condition. The main goal of this study is to propose efficient PSCs, using low-temperature processed ETM (SnO<sub>2</sub>) with other alternative efficient HTMs.

Here in, firstly, ETM will be optimized and for the second step through comparative study of three devices using TiO<sub>2</sub>, ZnO and SnO<sub>2</sub> as ETMs, MAPbI<sub>3</sub> as light harvester and Spiro-OMeTAD as HTM with the gold (Au) and FTO as back and front contact respectively was performed. The first step was executed through the screening of ETM, while the second step was focused on finding the efficient HTM using the configuration: FTO/SnO<sub>2</sub>/CH<sub>3</sub>NH<sub>3</sub>PbI<sub>3</sub>/HTM/Au. For this different HTM such as Spiro-OMeTAD poly(3-hexylthiophene-2,5-diyl) (P3HT), Copper antimony sulfide (CuSbS<sub>2</sub>), Cuprous oxide (Cu<sub>2</sub>O) and Copper thiocyanate (CuSCN) was simulated. The effect of different back contact on the device performance was also studied using SnO<sub>2</sub> as an ETM and CuSCN as HTM.

## 2. Device Simulation

The 1-dimensional Solar cell capacitance simulator (SCAPS) version. 3.3.07 was used as simulation platform (ELIS, University of Gent, Belgium). It is based on three coupled differential equations, namely, Poisson's (1) and continuity equations for holes (2) and electrons (3) as follows:

$$\frac{d}{dx} \left( \epsilon(x) \frac{d\Psi}{dx} \right) = q [ p(x) - n(x) + N_D^+(x) - N_A^-(x) + p_t(x) - n_t(x) ] \quad (1)$$

$$\frac{1}{j} \frac{dJ_p}{dx} + R_p(x) - G(x) = 0 \quad (2)$$

$$-\frac{1}{j} \frac{dJ_n}{dx} + R_n(x) - G(x) = 0 \quad (3)$$

Here,  $\epsilon$  is the permittivity,  $q$  is the charge of electron,  $\Psi$  is the electrostatic potential and  $n$  is electrons concentration,  $p$  is free hole concentration,  $n_t$  is trapped electron,  $p_t$  is trapped hole,  $N_D^+$  is the ionized donor-like doping and  $N_A^-$  is the ionized acceptor-like doping concentrations,  $R_n(x)$ ,  $R_p(x)$  are electrons and holes recombination rate,  $G(x)$  is the generation rate,  $J_n$  and  $J_p$  are the electron and hole current densities respectively.

Planar structure was used in this simulation, where the n-type transparent semi-conducting metal oxide was modelled by investigating ETM such as TiO<sub>2</sub>, ZnO and SnO<sub>2</sub>, CH<sub>3</sub>NH<sub>3</sub>PbI<sub>3</sub> used as light harvester, and Spiro-OMeTAD as HTM (Fig. 1a). Second part on this simulation was modelled by the SnO<sub>2</sub> as ETM with CH<sub>3</sub>NH<sub>3</sub>PbI<sub>3</sub> as absorber layer, using P3HT, CuSbS<sub>2</sub>,

$\text{Cu}_2\text{O}$ ,  $\text{CuSCN}$  and Spiro-OMeTAD as HTMs (Fig.1b). Moreover, the gold (Au) is used as the back contact and fluorine doped tin oxide (FTO) as the front contact.

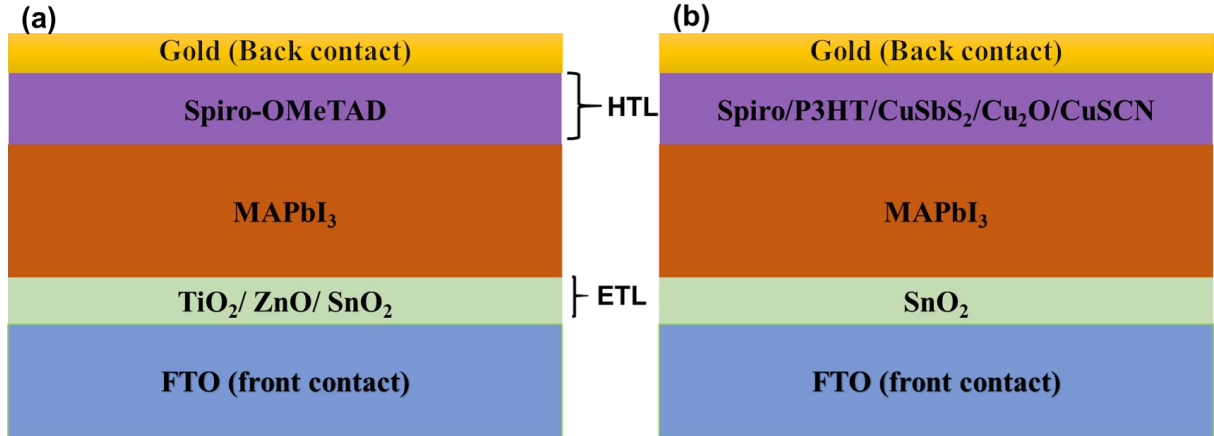


Figure 1 a & b. Device structure of simulated perovskite solar cell used in present study

The input parameters used in SCAPS-1D for simulation that are extracted from theories and literatures are summarized in Table 1. (Ahirrao et al., Anwar et al., Baumann et al., 2008; Behrouznejad et al., Fabregat-Santiago et al., Hussain et al., Khaliq et al., Laban and Etgar, 2013; Liu et al., 2014; Poplavskyy and Nelson, 2003; Stoumpos et al., 2013; Teimouri et al., Wang et al., 2009).

In the device simulation, ETM/ $\text{MAPbI}_3$  and  $\text{MAPbI}_3$ /HTM interface defect layer (IDL) are also introduced. The work function of HTM layers is calculated with respect to the valence band energy level (Anwar et al., 2017.) and input parameters are given in Table 2. Simulated current density-voltage (J-V) curve under illumination were obtained using standard AM 1.5G solar spectrum.

**Table1.** Simulation parameters of the perovskite solar cell, where  $\epsilon_r$  is dielectric constant,  $E_g$  is bandgap,  $\chi$  is electron affinity,  $N_c$  is effective conduction band density,  $N_v$  is effective valence band density,  $\mu_n$  is electron mobility and  $\mu_p$  is hole mobility,  $N_D$  is donor concentration while  $N_A$  is acceptor concentration,

Parameter	$\text{MAPbI}_3$	n-TiO <sub>2</sub>	n-SnO <sub>2</sub>	n-ZnO	Spiro-OMeTAD	P3HT	CuSbS <sub>2</sub>	Cu <sub>2</sub> O	CuSCN
thickness (nm)	450	Wide-range	Wide-range	Wide-range	Wide-range	Wide-range	Wide-range	Wide-range	Wide-range
$E_g$ (eV)	1.5	3.2	3.6	3.3	2.9	1.7	1.58	2.17	3.6
$\chi$ (eV)	3.93	4	4	4	2.2	3.5	4.2	3.2	1.7
$\epsilon_r$	30	100	9	9	3	3	14.6	7.1	10
$N_c$ (1/cm <sup>3</sup> )	$2.5 \times 10^{20}$	$1 \times 10^{21}$	$2.2 \times 10^{18}$	$3.7 \times 10^{18}$	$2.5 \times 10^{20}$	$2 \times 10^{21}$	$2 \times 10^{18}$	$2.5 \times 10^{18}$	$2.2 \times 10^{19}$
$N_v$ (1/cm <sup>3</sup> )	$2.5 \times 10^{20}$	$2 \times 10^{20}$	$1.8 \times 10^{19}$	$1.8 \times 10^{19}$	$2.5 \times 10^{20}$	$2 \times 10^{21}$	$1 \times 10^{19}$	$1.8 \times 10^{19}$	$1.8 \times 10^{18}$
$\mu_n$ (cm <sup>2</sup> /Vs)	50	0.006	100	100	0.0021	0.0018	49	200	100
$\mu_p$ (cm <sup>2</sup> /Vs)	50	0.006	0.256	25	0.0026	0.0186	49	8600	25

$N_A$ (1/cm <sup>3</sup> )	--	-	-	-	$1 \times 10^{18}$	$1 \times 10^{18}$	$1 \times 10^{18}$	$1 \times 10^{18}$	$1 \times 10^{18}$
$N_D$ (1/cm <sup>3</sup> )	--	$5.06 \times 10^{19}$	$1 \times 10^{17}$	$1 \times 10^{18}$	-	-	-	-	-
Work function (eV)		---	---	---	5	5.1	5.15	5.27	5.2

**Table 2.** Parameters of interface layer.

Interface	Defect type	Capture cross section electrons /holes (cm <sup>2</sup> )	Energetic distribution	Reference for defect energy level $E_t$	Total density (integrated over all energies) (1/cm <sup>2</sup> )	Total density (integrated over all energies) (1/cm <sup>2</sup> )
ETM/MAPbI <sub>3</sub>	Acceptor	$1 \times 10^{-17}$ $1 \times 10^{-18}$	Single	Above the VB maximum	0.32	$1 \times 10^9$
MAPbI <sub>3</sub> /HTM	Acceptor	$1 \times 10^{-18}$ $1 \times 10^{-19}$	Single	Above the VB maximum	0.07	$1 \times 10^9 - 1 \times 10^{12}$

### 3. Results and discussion

#### 3.1. Performance of PSCs based on Spiro-OMeTAD as HTM using different ETM

The role of ETM is to facilitate diffusion of the electrons from the photoexcited perovskite layer (MAPbI<sub>3</sub>) into the FTO glass and thus to the external circuit. Materials have most used in the common devices suffer from the high temperature processing which has a deleterious effect on the cost of PSCs fabrication. To address such challenges, two categories of ETMs, were compared in this work, one based on high processing temperature such as TiO<sub>2</sub>, while the other was based on ZnO and SnO<sub>2</sub>, which can be processed at low temperature. The photovoltaic parameters obtained from our simulation are presented in Table 3.

**Table 3.** Performance of PSCs with 90 nm thick ETM layers.

Device Architect	$J_{sc}$ (mA·cm <sup>-2</sup> )	$V_{oc}$ (mV)	FF (%)	PCE (%)
FTO/ZnO/MAPbI <sub>3</sub> /Spiro-OMeTAD/Au	25.10	1120	81.86	23.21
FTO/TiO <sub>2</sub> /MAPbI <sub>3</sub> /Spiro-OMeTAD/Au	24.98	1120	81.68	23.04
FTO/SnO <sub>2</sub> /MAPbI <sub>3</sub> /Spiro-OMeTAD/Au	25.59	1130	81.54	23.55

ETM thicknesses were kept same in all three different type of solar cells investigated. From the Table 3, it can be observed that for the same thickness of all the ETM, the efficiency of PSC based on SnO<sub>2</sub> as ETM was higher than of ZnO and TiO<sub>2</sub>. It can be deduced from Table 3 and  $J$ - $V$  curve in Figure 2 a and b, that the device based on SnO<sub>2</sub> as ETM showed higher current density than other ETMs employed here, due to increase light absorption by the perovskite, which also reflects in the EQE increment in the 300-450 nm spectral region. SnO<sub>2</sub> has a wider band gap (3.6 eV) and shows higher transmittance between 300-400 nm as compared to ZnO (3.3eV) and TiO<sub>2</sub> (3.2eV) (Huang et al., 2017; Ke et al., 2015; Khan et al., 2010; Martínez-Denegri et al., 2018; Pinpithak et al., 2017; Roose et al., 2016). These results suggest that low temperature processed SnO<sub>2</sub> as ETM in PSCs can be an effective candidate for efficient devices

fabrication. Our results are in accordance with the other reported experimental studies and numerical simulations (Adhikari et al., 2016; Anaraki et al., 2016; Guo et al., 2018; Huang et al., 2018.).

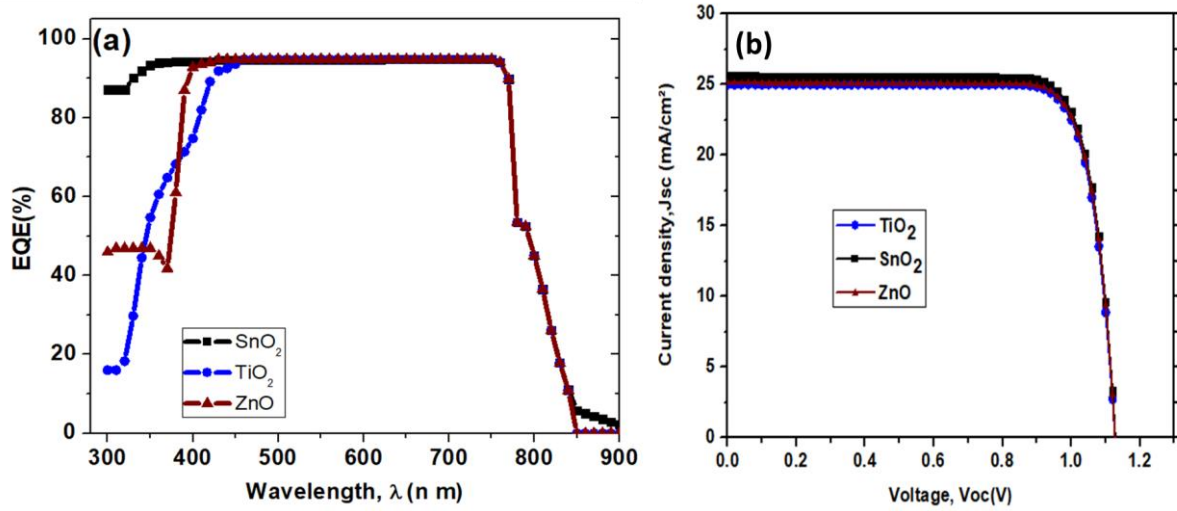


**Fig. 2.** a) Simulated EQE curves and b)  $J$ - $V$  curves of perovskite solar cells with 90 nm thick ZnO, TiO<sub>2</sub>, and SnO<sub>2</sub> ETL layer.

### 3.2. Effect of ETMs Thickness on photovoltaic parameters

Fig.3 shows the variation of PV parameters open circuit voltage ( $V_{oc}$ ), short circuit current density ( $J_{sc}$ ), fill factor ( $FF$ ) and PCE as a function of ETMs layer thickness. It is worth to note that in this simulation study, the highest donor dopant concentration ( $N_D$ ) was used for all the ETL layer and reported in Table 1. All the devices were simulated using MAPbI<sub>3</sub> (450 nm) as light harvester and Spiro-OMeTAD (400 nm) as HTM layer. The thickness of ETM layer used here was varied from 90 nm to 200 nm. It can be noted that with the increase of thickness >90 nm, led to decrease in  $V_{oc}$ ,  $J_{sc}$  and thus PCE in case of TiO<sub>2</sub> and ZnO, while in case of SnO<sub>2</sub>, there was no noticeable change in its value. It was found that TiO<sub>2</sub> was more affected than ZnO and SnO<sub>2</sub> due to its lower transmittance in 300-400 nm range and possesses low electron mobility, thus reduction in  $J_{sc}$  value occurs as a function of increased ETM thickness, which can be ascribed to the partial absorption of incident light by thicker TiO<sub>2</sub> and ZnO layer. Hence it decreases the rate of charge generation and collection and consequently short circuit current ( $J_{sc}$ ) decreases (Adhikari et al., 2016; Kirchartz et al., 2012). However, in case of SnO<sub>2</sub>, due to its high transparency, active layer absorption is less affected and  $J_{sc}$  did not decrease significantly up to a certain thickness of 150 nm thus rate of charge generation rate increases as compared to the recombination. Moreover, due to high carrier mobility and high carrier concentration of SnO<sub>2</sub>, the series resistance decreases with the thickness due to increase in conductivity and thus fill factor also increases up to certain thickness of 150 nm and beyond this insignificant changes occurs.

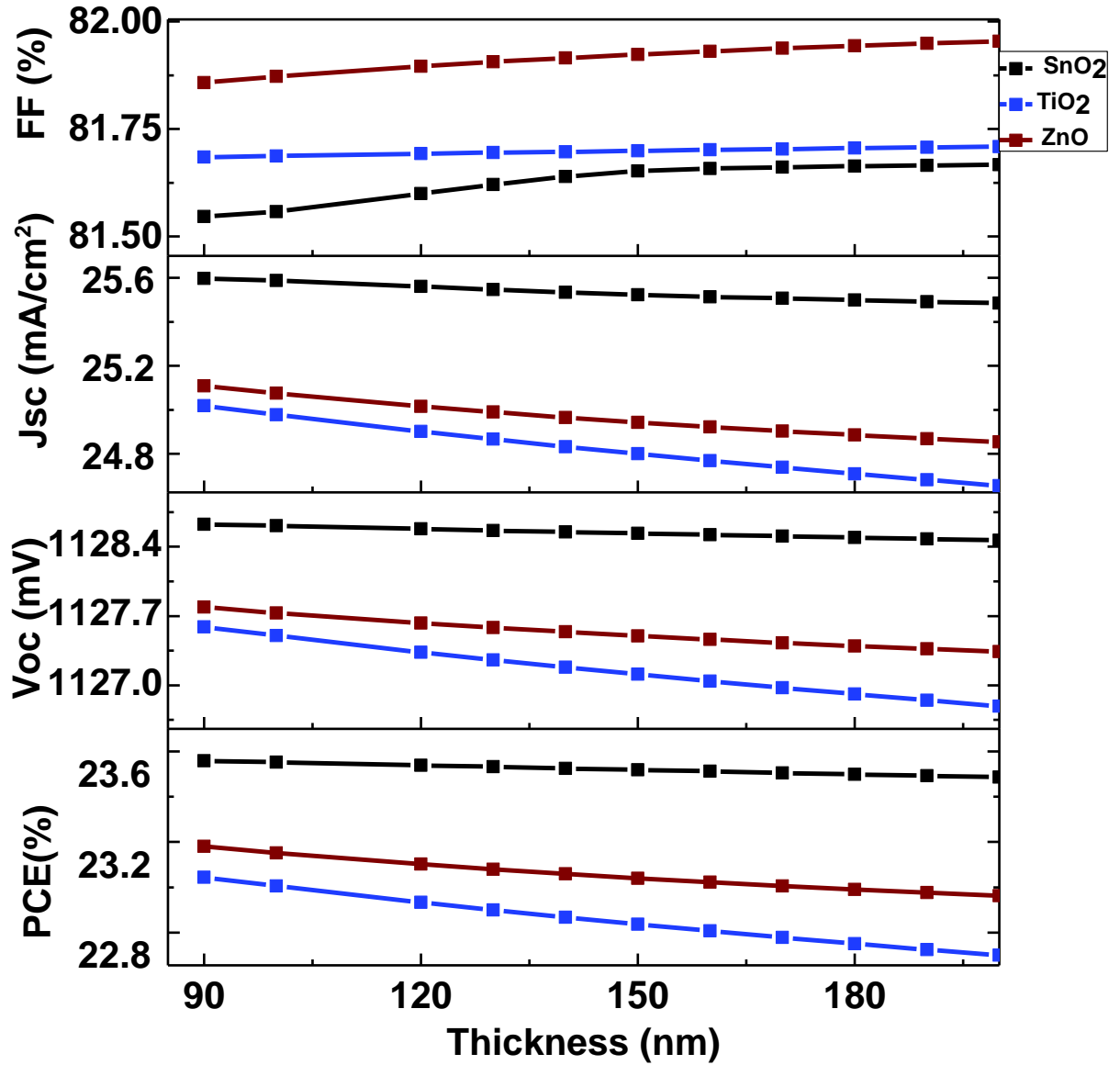


**Fig. 3.** Effect of different ETM thickness on photovoltaic parameters of MAPbI<sub>3</sub> based planar perovskite solar cells using Spiro-OMeTAD as HTM.

It is worthy to mention, that we have used high donor dopant concentration ( $N_D$ ) for ETLs and as in previous reports ([Adhikari et al., 2016](#); [Kirchartz et al., 2012](#)). The high value of donor dopant concentration ( $N_D$ ) for ETLs leads to increase the conductivity of ETLs and reduces the resistivity and thus fill factor. Similar observation was seen in organic solar cells that FF increases with high  $N_D$  and vice versa ([Trukhanov et al., 2011](#)). For better understanding, the effect of ETLs thickness on the fill factor as a function of dopant concentration ( $N_D$ ) was investigated (Figure 4a-c). We noted that with low  $N_D$ , the fill factor become very sensitive to high thickness. If we increased the thickness of ETLs the fill factor drops inversely to high  $N_D$  (Fig.4 a-c), due to improvement in the conductivity of ETLs as mentioned above. Thus for high value of  $N_D$ , the FF is less or independent up to certain thickness.

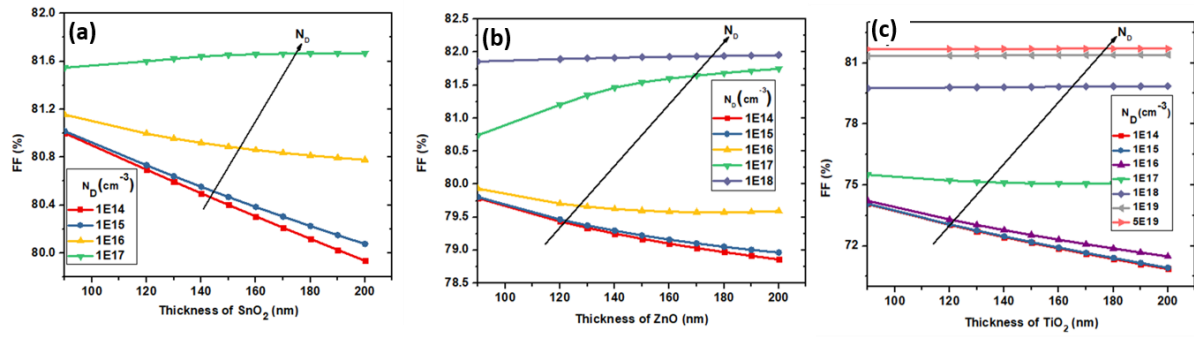


Figure 4. The effect of ETLs thickness a)  $\text{SnO}_2$ , b)  $\text{ZnO}$  and c)  $\text{TiO}_2$  on the fill factor as a function of dopant donor concentration ( $N_D$ ).

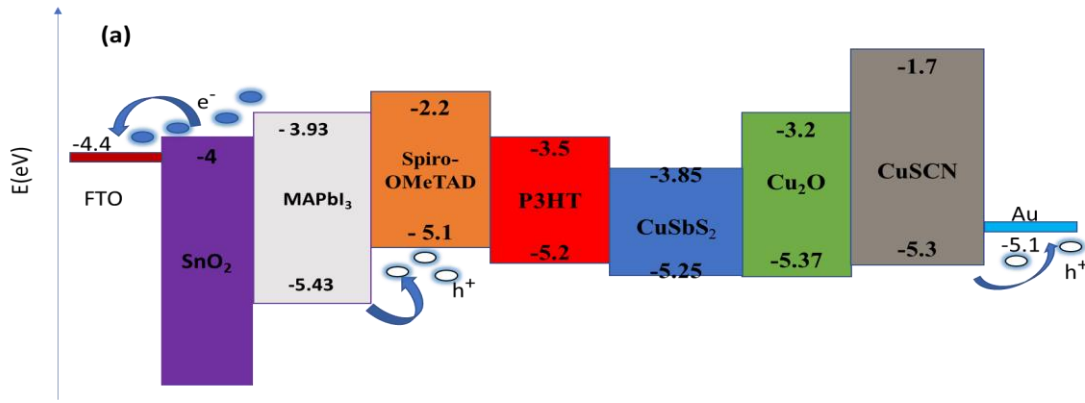
#### 4. Solar cell performance with $\text{SnO}_2$ ETM and using different HTMs

##### 4.1. Photovoltaic parameters

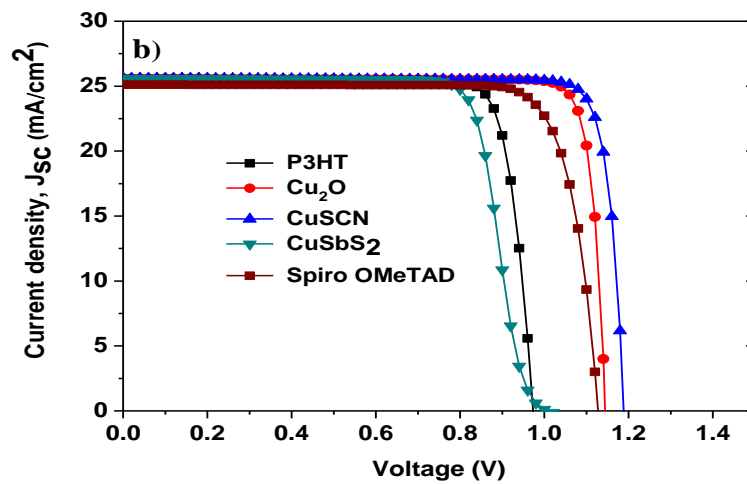
Figure 5a shows the energy level diagrams of PSCs using  $\text{SnO}_2$  as ETM and different inorganic and organic HTM which affect the valence band offset (i.e. the difference between the valence band of the HTM and of the absorber layer). The energy level alignment plays an important role in the high performance of the solar cells. The photo generated electrons in the perovskite are injected to the  $\text{SnO}_2$  conduction band and hole to the HTM and then these extracted electrons and holes are collected to their respective front (FTO) and back contact (Au metal) respectively. To extract the electron at  $\text{SnO}_2/\text{MAPbI}_3$  interface, the electron affinity (E.A.) of  $\text{SnO}_2$  should be higher than of perovskite and to extract the holes at HTM/  $\text{MAPbI}_3$  interface, the ionization energy (I.E.) of HTM should be lower than of perovskite. The energy level mismatching at ETM/perovskite and perovskite/HTM interface influence the PV properties more importantly, open circuit voltage ( $V_{oc}$ ) and short circuit current ( $J_{sc}$ ).

Fig 5b and Table 4 illustrates simulated  $J$ - $V$  curves of PSCs based on  $\text{MAPbI}_3$  as perovskite (thickness 450 nm),  $\text{SnO}_2$  as ETM (thickness 90 nm) with P3HT,  $\text{CuSbS}_2$ ,  $\text{Cu}_2\text{O}$ ,  $\text{CuSCN}$  and Spiro-OMeTAD as HTMs. It can be deduced that the devices fabricated with  $\text{CuSCN}$  as HTM outperformed and gave a  $V_{oc}$  of 1190 mV,  $J_{sc}$  of  $25.60 \text{ mA/cm}^2$  and FF of 87.85% with an overall PCE of 26.74% can be achieved. This was followed by  $\text{Cu}_2\text{O}$ , which showed high performance after  $\text{CuSCN}$  with PCE of 25.97%,  $J_{sc}$  of  $25.61 \text{ mA/cm}^2$ ,  $V_{oc}$  of 1150 mV and FF of 88.39%.  $\text{Cu}_2\text{O}$ , P3HT also gave promising results achieving PCE of 20.8% with  $V_{oc}$  of 1140 mV,  $J_{sc}$  of  $25.55 \text{ mA/cm}^2$  and FF of 77.88%. The relatively low PV performance was found when  $\text{CuSbS}_2$  was used as HTM which gave a PCE of 19.88%,  $V_{oc}$  960 mV,  $J_{sc}$  of  $25.59 \text{ mA/cm}^2$  and FF of 77.88%. The values of the energy levels of the layers used in the simulation with  $\text{SnO}_2$  as ETM are illustrated in Fig.5 a.

Among all the HTMs simulated here, the best PV performance was noted with  $\text{CuSCN}$  followed by  $\text{Cu}_2\text{O}$  as HTMs in PSCs using  $\text{SnO}_2$  as ETM. These two upright performing HTMs have deeper valence band energy level with respect to  $\text{MAPbI}_3$  perovskite absorber compared with other HTMs, which allowed to maximize the  $V_{oc}$ , and large optical band gap ( $E_g = 3.6\text{eV}$ ) of  $\text{CuSCN}$  guarantees high electron blocking properties to prevent photogenerated electrons transfer from perovskite to itself. Further it's optical transparency in UV-visible region allow to increase the absorption in absorbing layer and thus enhanced the short circuit current (Calió et al., 2016b, 2016a; Madhavan et al., 2016)



**Figure 5. a)** Corresponding band energy diagrams of planar perovskite solar cells using  $\text{SnO}_2$  as ETM and different HTM



**Figure 5. b)** Simulated  $J$ - $V$  curves of perovskite solar cells using  $\text{SnO}_2$  as ETM and P3HT,  $\text{CuSbS}_2$ ,  $\text{Cu}_2\text{O}$ ,  $\text{CuSCN}$  and Spiro-OMeTAD as different HTM.

#### 4.2. Effect of HTMs thickness on photovoltaic parameters

Fig 6a-e depicts the influence of HTMs thickness in the range of 20-200 nm on PV parameters with various HTMs, Spiro-OMeTAD, P3HT,  $\text{CuSbS}_2$ ,  $\text{Cu}_2\text{O}$  and  $\text{CuSCN}$  with  $\text{SnO}_2$  and  $\text{MAPbI}_3$  as ETM and absorber layer respectively. These results suggest that PV parameters depends on the type and thickness of HTM used. The optimization of HTM thickness is paramount not only to improve the performance but also this HTM layer act as capping layer and prevent direct contact between the perovskite and cathode. It can be deduced from the Fig 5a-e, in case of thickness exceeds 100 nm, the PCE decreases (in case of Spiro-OMeTAD and P3HT) or showed negligible changes in case of  $\text{CuSbS}_2$ ,  $\text{Cu}_2\text{O}$ , and  $\text{CuSCN}$ . For the same thickness,  $V_{oc}$  increases in case of Spiro-OMeTAD,  $\text{Cu}_2\text{O}$ , and  $\text{CuSCN}$  and showed low  $V_{oc}$  with rest of HTMs ( $\text{CuSbS}_2$ , P3HT). The  $FF$  increases dramatically (Spiro-OMeTAD, P3HT and  $\text{CuSbS}_2$ ) or with negligible value, finally  $J_{sc}$  showed a very small increment (in case of  $\text{Cu}_2\text{O}$ ) or a decrease in other HTMs.

The P3HT and Spiro-OMeTAD possesses low conductivity and low charge carrier mobilities as compared to the inorganic HTMs. Thus increased thickness in case of organic HTMs will increase the resistance of the layer and consequently, it will decrease the fill factor ( $FF$ ) due to lower mobility, rate of recombination will be higher and thus will yield poor device performance. While in case of inorganic HTMs, due to their high mobility and high conductivity, thickness does not play an important role. Taiho Park co-workers (Kim et al.,

2015) also showed experimentally optimization of HTL layer and discovered that a thicker HTL with high mobility can provide high performance and reproducibility.

Table 4. Summary of the photovoltaic parameters for planar perovskite solar cells using optimized SnO<sub>2</sub> ETL thickness (90 nm) and optimized HTM thickness for maximum light harvesting. Based on the results illustrated in Table 4, we can speculate that all the devices perform effectively when the thickness was 100 nm, on contrary with literature value where 400 nm was simulated.

**Table 4.** Performance of SnO<sub>2</sub>-PSC with different HTM with optimum thickness.

Device Architect	HTM thickness (nm)	PCE (%)	V <sub>oc</sub> (mV)	J <sub>sc</sub> (mA/cm <sup>2</sup> )	FF (%)
FTO/SnO <sub>2</sub> /MAPbI <sub>3</sub> /Spiro-OMeTAD/Au	100	24.18	1130	25.60	83.50
FTO/SnO <sub>2</sub> /MAPbI <sub>3</sub> /P3HT/Au	100	21.52	970	25.56	86.52
FTO/SnO <sub>2</sub> /MAPbI <sub>3</sub> /CuSbS <sub>2</sub> /Au	100	19.70	960	25.59	80.18
FTO/SnO <sub>2</sub> /MAPbI <sub>3</sub> /Cu <sub>2</sub> O/Au	100	25.97	1140	25.61	88.59
FTO/SnO <sub>2</sub> /MAPbI <sub>3</sub> /CuSCN/Au	100	26.74	1190	25.61	87.81

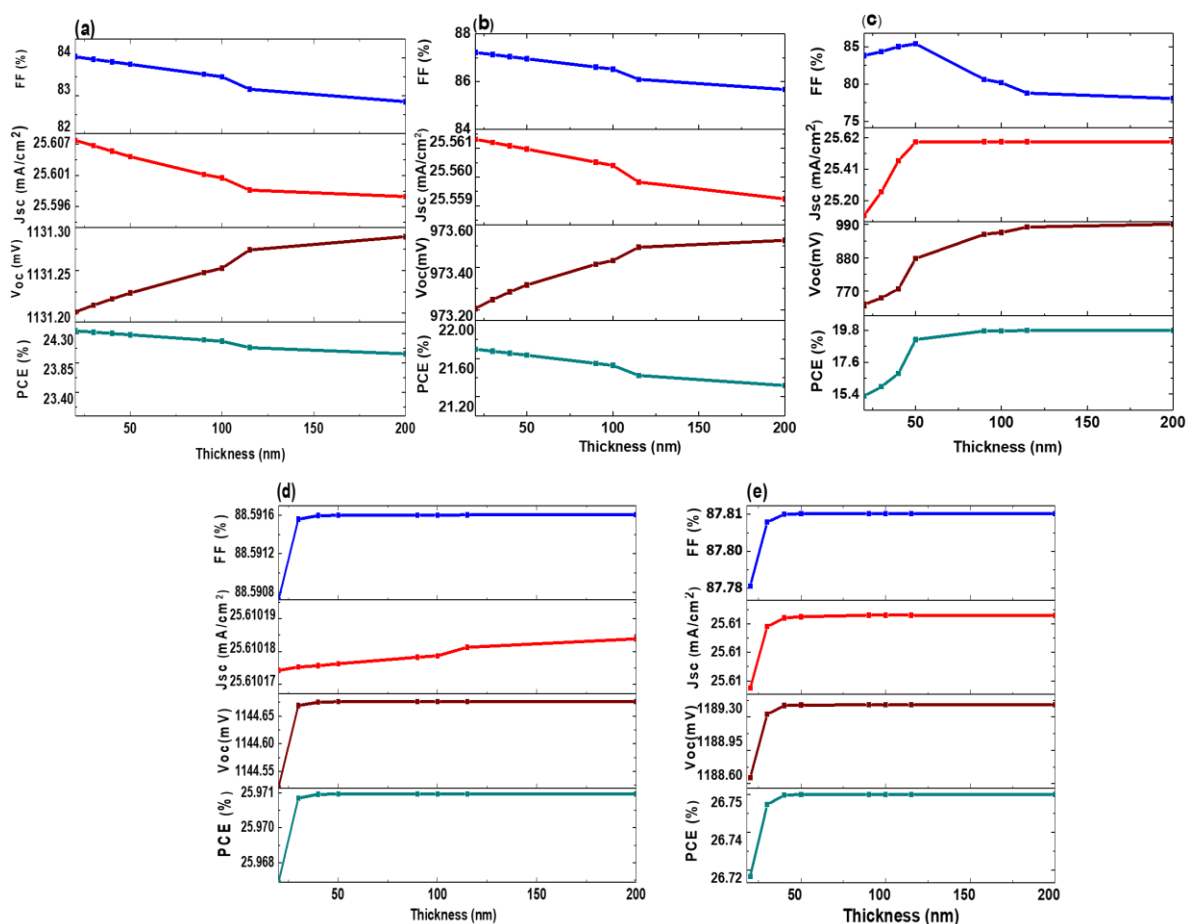


**Figure 6.** Effect of HTM thickness on photovoltaic parameters in n-i-p configuration using SnO<sub>2</sub> (90nm) as ETL in MAPbI<sub>3</sub> based perovskite solar cells; a) Spiro-OMeTAD, b) P3HT, c) CuSbS<sub>2</sub>, d) Cu<sub>2</sub>O and e) CuSCN.

## 5. Impact of work function of back contact on the PCE of $\text{SnO}_2$ -PSCs with CuSCN as HTM

To further optimize each stacking in PSCs, we have simulated the PSCs with different back contact in the device configuration of  $\text{FTO}/\text{SnO}_2/\text{MAPbI}_3/\text{CuSCN}/\text{back contact}$  (adaptable), to ratify whether another alternate back-contact (cathode) with similar performance as of Au can be used. Figure 7 showed the PCE of our simulated solar cell containing different back contact such as Ag (4.74eV), Fe (4.81eV), C (5eV), Au (5.1), Ni (5.5eV) and Pt (5.70eV). The PCE of PSCs first increases with increasing the work function of metals up to a certain value of  $\sim 5.2$  eV then it saturates at 5.4 eV that might be related to the work function of CuSCN ( $\sim 5.2$  eV), the start of saturation in the efficiency was observed due to the alignment with the work function of HTM and the valence band of the absorber layer. With high metal work function, the fermi level energy decreases due to band bending at the metal-semiconductor interface, leading the contact more ohmic (Behrouznejad et al., 2016). From these values of metal work function, illustrated in Figure 8 for different back contacts, we can confirm that the carbon with work function at 5eV, can be used as an effective alternative to replace the expensive Au electrode, and an efficiency of 25.55%, can be achieved using the structure  $\text{FTO}/\text{SnO}_2/\text{MAPbI}_3/\text{CuSCN}/\text{C}$  for low cost PSCs.

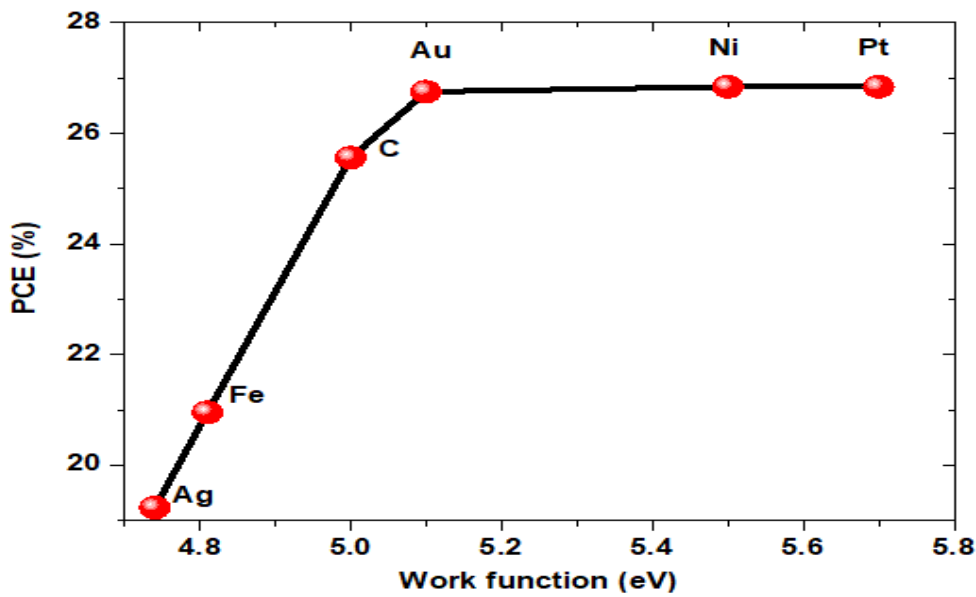


**Figure 7.** Effect of work function of different back contact (metal contact) on the power conversion efficiency of planar perovskite solar cells,  $\text{MAPbI}_3$  as perovskite absorber,  $\text{SnO}_2$  as ETM and CuSCN as HTM.

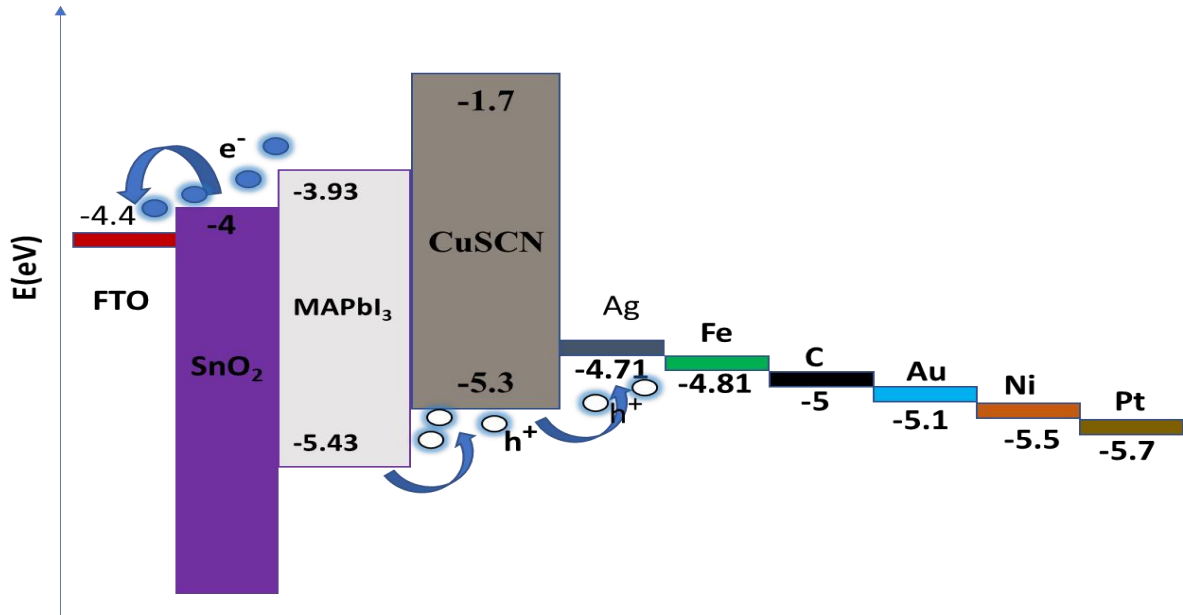


**Figure 8.** Energy levels for different back contacts with SnO<sub>2</sub>, MAPbI<sub>3</sub> and CuSCN.

## 6. CONCLUSION

To summarize, performance of planar PSC with SnO<sub>2</sub> as ETM was studied and a comparative study was made using other conventional ETMs and HTMs through a numeral simulation by SCAPS package for the first time. These results illustrated that the application of SnO<sub>2</sub> as an alternative ETM holds great promise in terms of PV performance as compared with TiO<sub>2</sub> and ZnO in the device architecture FTO/ETM/MAPbI<sub>3</sub>/Spiro-OMeTAD/Au, and PCE of 23.21 %, 23.04 % and 23.55% can be simulated using ZnO, TiO<sub>2</sub> and SnO<sub>2</sub> respectively. Additionally, the effect of various organic and inorganic HTMs such as, P3HT, CuSbS<sub>2</sub>, Cu<sub>2</sub>O and CuSCN on the PV parameters was also studied and it was found that the PCE improved from 23.55% to 26.74 % and  $V_{oc}$  from 1130 mV to 1180 mV, when Spiro-OMeTAD was substituted by CuSCN as HTM. In order to reduce the cost of fabricated PSCs, the effect of ETM and HTM thickness was simulated, which suggest that by employing low thickness in range of 30 -100 nm of HTMs can produce similar or high performance compared with 400 nm reported in literature. Further, by using the carbon as back contact can allow achieving a PCE of 25.25 %, which is a model material to replace the expensive gold electrode (Au). Our results will pave way to optimize the PSCs cost and performance.

## Acknowledgment

This work has received funding from the European Union Seventh H2020 Programme under European Research council Consolidator grant [MOLEMAT, 72630]. We would like to express sincere thanks to Dr. Marc Burgelman, Department of Electronics and Information Systems (ELIS), University of Gent, Belgium, for providing the SCAPS-1D simulation tool.

## References

- Adhikari, K.R., Gurung, S., Bhattarai, B.K., Soucase, B.M., 2016. Comparative study on MAPbI<sub>3</sub> based solar cells using different electron transporting materials. *physica status solidi (c)* 13, 13–17.
- Ahirrao, P. B., Gosavi, S. R., Sonawane, S. S., & Patil, R. S. (2011). Wide band gap nanocrystalline CuSCN thin films deposited by modified chemical method. *Arch. Phys. Res*, 2(3), 29-33.
- Anaraki, E.H., Kermanpur, A., Steier, L., Domanski, K., Matsui, T., Tress, W., Saliba, M., Abate, A., Grätzel, M., Hagfeldt, A., 2016. Highly efficient and stable planar perovskite solar cells by solution-processed tin oxide. *Energy & Environmental Science* 9, 3128–3134.
- Anwar, F., Mahbub, R., Satter, S. S., & Ullah, S. M. (2017). Effect of Different HTM Layers and Electrical Parameters on ZnO Nanorod-Based Lead-Free Perovskite Solar Cell for High-Efficiency Performance. *International Journal of Photoenergy*, 2017.
- Baena, J.P.C., Steier, L., Tress, W., Saliba, M., Neutzner, S., Matsui, T., Giordano, F., Jacobsson, T.J., Kandada, A.R.S., Zakeeruddin, S.M., 2015. Highly efficient planar perovskite solar cells through band alignment engineering. *Energy & Environmental Science* 8, 2928–2934.
- Baumann, A., Lorrman, J., Deibel, C., Dyakonov, V., 2008. Bipolar charge transport in poly(3-hexyl thiophene)/methanofullerene blends: A ratio dependent study. *Applied Physics Letters* 93, 252104.
- Behrouznejad, F., Shahbazi, S., Taghavinia, N., Wu, H. P., & Diao, E. W. G. (2016). A study on utilizing different metals as the back contact of CH<sub>3</sub>NH<sub>3</sub>PbI<sub>3</sub> perovskite solar cells. *Journal of Materials Chemistry A*, 4(35), 13488-13498.
- NREL, 2019, Solar cell efficiency chart. <https://www.nrel.gov/pv/assets/pdfs/pv-efficiencies-08-02-2019>.
- Burschka, J., Pellet, N., Moon, S.-J., Humphry-Baker, R., Gao, P., Nazeeruddin, M.K., Grätzel, M., 2013. Sequential deposition as a route to high-performance perovskite-sensitized solar cells. *Nature* 499, 316.
- Calió, L., Kazim, S., Grätzel, M., Ahmad, S., 2016a. Hole-Transport Materials for Perovskite Solar Cells. *Angewandte Chemie - International Edition* 55, 14522–14545.
- Calió, L., Kazim, S., Grätzel, M., Ahmad, S., 2016b. Lochtransportmaterialien für Perowskit-Solarzellen. *Angewandte Chemie* 128, 14740–14764. 7
- Calió, L., Momblona, C., Gil-Escrig, L., Kazim, S., Sessolo, M., Sastre-Santos, Á., Bolink, H.J., Ahmad, S., 2017. Vacuum deposited perovskite solar cells employing dopant-free triazatruxene as the hole transport material. *Solar Energy Materials and Solar Cells* 163, 237–241.
- Cogal, S., Calio, L., Celik Cogal, G., Salado, M., Kazim, S., Oksuz, L., Ahmad, S., Uygun Oksuz, A., 2018. RF plasma-enhanced graphene–polymer composites as hole transport materials for perovskite solar cells. *Polymer Bulletin* 75, 4531–4545.
- Di, Y., Zeng, Q., Huang, C., Tang, D., Sun, K., Yan, C., Wang, Y., Ke, S., Jiang, L., Hao, X., Lai, Y., Liu, F., 2018. Thermal-evaporated selenium as a hole-transporting material for

- planar perovskite solar cells. *Solar Energy Materials and Solar Cells* 185, 130–135.
- Eperon, G.E., Stranks, S.D., Menelaou, C., Johnston, M.B., Herz, L.M., Snaith, H.J., 2014. Formamidinium lead trihalide: a broadly tunable perovskite for efficient planar heterojunction solar cells. *Energy & Environmental Science* 7, 982–988.
- Fabregat-Santiago, F., Randriamahazaka, H., Zaban, A., Garcia-Canadas, J., Garcia-Belmonte, G., & Bisquert, J. (2006). Chemical capacitance of nanoporous-nanocrystalline TiO<sub>2</sub> in a room temperature ionic liquid. *Physical Chemistry Chemical Physics*, 8(15), 1827-1833.
- Garza, C., Shaji, S., Arato, A., Perez Tijerina, E., Alan Castillo, G., Das Roy, T.K., Krishnan, B., 2011. P-Type CuSbS<sub>2</sub> thin films by thermal diffusion of copper into Sb<sub>2</sub>S<sub>3</sub>. *Solar Energy Materials and Solar Cells* 95, 2001–2005.
- Gong, J., Darling, S. B., & You, F. (2015). Perovskite photovoltaics: life-cycle assessment of energy and environmental impacts. *Energy & Environmental Science*, 8(7), 1953-1968.
- Green, M.A., 1982. Accuracy of analytical expressions for solar cell fill factors. *Solar Cells* 7, 337–340.
- Guo, X., Dong, H., Li, W., Li, N., Wang, L., 2015. Multifunctional MgO layer in perovskite solar cells. *ChemPhysChem* 16, 1727–1732.
- Guo, Y., Jiang, J., Zuo, S., Shi, F., Tao, J., Hu, Z., ... & Chu, J. (2018). RF sputtered CdS films as independent or buffered electron transport layer for efficient planar perovskite solar cell. *Solar Energy Materials and Solar Cells*, 178, 186-192..
- Hossain, M.I., Alharbi, F.H., Tabet, N., 2015. Copper oxide as inorganic hole transport material for lead halide perovskite based solar cells. *Solar Energy* 120, 370–380.
- Huang, X., Hu, Z., Xu, J., Wang, P., Wang, L., Zhang, J., Zhu, Y., 2017. Low-temperature processed SnO<sub>2</sub> compact layer by incorporating TiO<sub>2</sub> layer toward efficient planar heterojunction perovskite solar cells. *Solar Energy Materials and Solar Cells* 164, 87–92.
- Huang, Z., Wang, D., Wang, S., & Zhang, T. (2018). Highly Efficient and Stable MAPbI<sub>3</sub> Perovskite Solar Cell Induced by Regulated Nucleation and Ostwald Recrystallization. *Materials*, 11(5), 778..
- Hussain, A., Ahmed, R., Ali, N., Butt, F. K., Shaari, A., Shamsuri, W. W., & Verma, K. D. (2016). Post annealing effects on structural, optical and electrical properties of CuSbS<sub>2</sub> thin films fabricated by combinatorial thermal evaporation technique. *Superlattices and Microstructures*, 89, 136-144.
- Kazim, S., Nazeeruddin, M.K., Grätzel, M., Ahmad, S., 2014. Perovskite as light harvester: A game changer in photovoltaics. *Angewandte Chemie - International Edition* 53, 2812–2824.
- Ke, W., Fang, G., Liu, Q., Xiong, L., Qin, P., Tao, H., Wang, J., Lei, H., Li, B., Wan, J., 2015a. Low-temperature solution-processed tin oxide as an alternative electron transporting layer for efficient perovskite solar cells. *Journal of the American Chemical Society* 137, 6730–6733.
- Ke, W., Fang, G., Liu, Q., Xiong, L., Qin, P., Tao, H., Wang, J., Lei, H., Li, B., Wan, J., Yang, G., Yan, Y., 2015b. Low-Temperature Solution-Processed Tin Oxide as an Alternative Electron Transporting Layer for Efficient Perovskite Solar Cells. *Journal of the American Chemical Society* 137, 6730–6733.

- Khaliq, A., Xue, F. L., & Varahramyan, K. (2009). Numerical simulation of spin coated P3HT organic thin film transistors with field dependent mobility and distributed contact resistance. *Microelectronic Engineering*, 86(11), 2312-2315.
- Khan, A.F., Mehmood, M., Aslam, M., Ashraf, M., 2010. Characteristics of electron beam evaporated nanocrystalline SnO<sub>2</sub> thin films annealed in air. *Applied Surface Science* 256, 2252–2258.
- Kim, G.W., Shinde, D. V., Park, T., 2015. Thickness of the hole transport layer in perovskite solar cells: Performance versus reproducibility. *RSC Advances* 5, 99356–99360.
- Kirchartz, T., Agostinelli, T., Campoy-Quiles, M., Gong, W., Nelson, J., 2012. Understanding the Thickness-Dependent Performance of Organic Bulk Heterojunction Solar Cells: The Influence of Mobility, Lifetime, and Space Charge. *The Journal of Physical Chemistry Letters* 3, 3470–3475.
- Koh, T.M., Fu, K., Fang, Y., Chen, S., Sum, T.C., Mathews, N., Mhaisalkar, S.G., Boix, P.P., Baikie, T., 2013. Formamidinium-containing metal-halide: an alternative material for near-IR absorption perovskite solar cells. *The Journal of Physical Chemistry C* 118, 16458–16462.
- Kojima, A., Teshima, K., Shirai, Y., Miyasaka, T., 2009. Organometal halide perovskites as visible-light sensitizers for photovoltaic cells. *Journal of the American Chemical Society* 131, 6050–6051.
- Laban, W.A., Etgar, L., 2013. Depleted hole conductor-free lead halide iodide heterojunction solar cells. *Energy & Environmental Science* 6, 3249–3253.
- Leijtens, T., Eperon, G.E., Pathak, S., Abate, A., Lee, M.M., Snaith, H.J., 2013. Overcoming ultraviolet light instability of sensitized TiO<sub>2</sub> with meso-superstructured organometal tri-halide perovskite solar cells. *Nature communications* 4, 2885.
- Lin, Q., Armin, A., Nagiri, R.C.R., Burn, P.L., Meredith, P., 2015. Electro-optics of perovskite solar cells. *Nature Photonics* 9, 106.
- Liu, D., Kelly, T.L., 2014. Perovskite solar cells with a planar heterojunction structure prepared using room-temperature solution processing techniques. *Nature photonics* 8, 133.
- Liu, F., Zhu, J., Wei, J., Li, Y., Lv, M., Yang, S., Zhang, B., Yao, J., Dai, S., 2014. Numerical simulation: Toward the design of high-efficiency planar perovskite solar cells. *Applied Physics Letters* 104, 253508.
- Madhavan, V.E., Zimmermann, I., Roldán-Carmona, C., Grancini, G., Buffiere, M., Belaidi, A., Nazeeruddin, M.K., 2016. Copper Thiocyanate Inorganic Hole-Transporting Material for High-Efficiency Perovskite Solar Cells. *ACS Energy Letters* 1, 1112–1117.
- Martínez-Denegri, G., Colodrero, S., Kramarenko, M., Martorell, J., 2018. All-Nanoparticle SnO<sub>2</sub>/TiO<sub>2</sub> Electron-Transporting Layers Processed at Low Temperature for Efficient Thin-Film Perovskite Solar Cells. *ACS Applied Energy Materials* acae.8b01118.
- Pinpithak, P., Chen, H.-W., Kulkarni, A., Sanehira, Y., Ikegami, M., Miyasaka, T., 2017. Low-temperature and Ambient Air Processes of Amorphous SnO<sub>x</sub>-based Mixed Halide Perovskite Planar Solar Cell. *Chemistry Letters* 46, 382–384.
- Poplavskyy, D., Nelson, J., 2003. Nondispersive hole transport in amorphous films of methoxy-spirofluorene-arylamine organic compound. *Journal of Applied Physics* 93, 341–346.

- Qin, P., Tanaka, S., Ito, S., Tetreault, N., Manabe, K., Nishino, H., Nazeeruddin, M.K., Grätzel, M., 2014. Inorganic hole conductor-based lead halide perovskite solar cells with 12.4% conversion efficiency. *Nature Communications* 5, 1–6.
- Reyna, Y., Salado, M., Kazim, S., Pérez-Tomas, A., Ahmad, S., Lira-Cantu, M., 2016. Performance and stability of mixed FAPbI<sub>3</sub>(0.85)MAPbBr<sub>3</sub>(0.15) halide perovskite solar cells under outdoor conditions and the effect of low light irradiation. *Nano Energy* 30, 570–579.
- Roose, B., Baena, J.-P.C., Gödel, K.C., Graetzel, M., Hagfeldt, A., Steiner, U., Abate, A., 2016. Mesoporous SnO<sub>2</sub> electron selective contact enables UV-stable perovskite solar cells. *Nano Energy* 30, 517–522.
- Salado, M., Calió, L., Contreras-Bernal, L., Idígoras, J., Anta, J.A., Ahmad, S., Kazim, S., 2018. Understanding the influence of interface morphology on the performance of perovskite solar cells. *Materials* 11, 1–13.
- Salado, M., Kazim, S., Nazeeruddin, M.K., Ahmad, S., 2019. Appraisal of Crystal Expansion in CH<sub>3</sub>NH<sub>3</sub>PbI<sub>3</sub> on Doping: Improved Photovoltaic Properties. *ChemSusChem* 1–8.
- Salado, M., Oliva-Ramirez, M., Kazim, S., González-Elipé, A.R., Ahmad, S., 2017. 1-dimensional TiO<sub>2</sub> nano-forests as photoanodes for efficient and stable perovskite solar cells fabrication. *Nano Energy* 35, 215–222.
- Salmani, E., Laghrissi, A., Lamouri, R., Rouchdi, M., Dehmani, M., Ez-Zahraouy, H., Hassanain, N., Mzerd, A., Benyoussef, A., 2018. Theoretical study of electronic, magnetic and optical properties of TM (V, Cr, Mn and Fe) doped SnO<sub>2</sub>: ab-initio and Monte Carlo simulation. *Optical and Quantum Electronics* 50, 1–11.
- Shang, X., Wang, Z., Li, M., Zhang, L., Fang, J., Tai, J., He, Y., 2014. A numerical simulation study of CuInS<sub>2</sub> solar cells. *Thin Solid Films* 550, 649–653.
- Stoumpos, C.C., Malliakas, C.D., Kanatzidis, M.G., 2013. Semiconducting tin and lead iodide perovskites with organic cations: phase transitions, high mobilities, and near-infrared photoluminescent properties. *Inorganic chemistry* 52, 9019–9038.
- Sun, Q., Gong, X., Li, H., Liu, S., Zhao, X., Shen, Y., Wang, M., 2018. Direct formation of I<sup>3-</sup> ions in organic cation solution for efficient perovskite solar cells. *Solar Energy Materials and Solar Cells* 185, 111–116.
- Teimouri, R., Microstructures, R.M.-S. and, 2018, U., 2018. Potential application of CuSbS<sub>2</sub> as the hole transport material in perovskite solar cell: A simulation study. *Superlattices and Microstructures* 118, 116–122.
- Trukhanov, V.A., Bruevich, V. V., Paraschuk, D.Y., 2011. Effect of doping on performance of organic solar cells. *PHYSICAL REVIEW B* 84, 205318.
- Wang, M., Grätzel, C., Moon, S., Humphry-Baker, R., Rossier-Iten, N., Zakeeruddin, S.M., Grätzel, M., 2009. Surface design in solid-state dye sensitized solar cells: effects of zwitterionic co-adsorbents on photovoltaic performance. *Advanced Functional Materials* 19, 2163–2172.
- Wang, M., Zang, Z., Yang, B., Hu, X., Sun, K., Sun, L., 2018. Performance improvement of perovskite solar cells through enhanced hole extraction: The role of iodide concentration gradient. *Solar Energy Materials and Solar Cells* 185, 117–123.

- Yu, W., Li, F., Wang, H., Alarousu, E., Chen, Y., Lin, B., Wang, L., Hedhili, M.N., Li, Y., Wu, K., Wang, X., Mohammed, O.F., Wu, T., 2016. Ultrathin Cu<sub>2</sub>O as an efficient inorganic hole transporting material for perovskite solar cells. *Nanoscale* 8, 6173–6179.
- Zhou, J., Bian, G.Q., Zhu, Q.Y., Zhang, Y., Li, C.Y., Dai, J., 2009. Solvothermal crystal growth of CuSbQ<sub>2</sub> (Q=S, Se) and the correlation between macroscopic morphology and microscopic structure. *Journal of Solid State Chemistry* 182, 259–264.